

Original Article

Modal Analysis of Strong Resonance in Multi-Machine System with Power System Stabilizer

Jarapala Siva Naik¹, R. Thirumalaivasan²

^{1,2}School of Electrical Engineering, Vellore Institute of Technology, TamilNadu, India.

²Corresponding Author : thirumalai.r@vit.ac.in

Received: 15 November 2023

Revised: 05 December 2023

Accepted: 15 January 2024

Published: 16 February 2024

Abstract - When two or more control parameters of a power system are altered concurrently, their improper settings may lead to strong resonance due to a modal interaction. The research focuses on the design of a Power System Stabilizer (PSS) to address this instability in multi-machine power systems. To investigate the phenomenon of strong resonance, a test system of a 3-machine, 10-bus power system with a single PSS is utilized. Both full-order and reduced-order mathematical models of the system are employed for analysis. The full-order model is leveraged for eigenvalue and participation factor analyses, aiding in PSS performance evaluation and root locus visualization. Meanwhile, the reduced-order model, obtained through multi-modal decomposition, allows for examining strong resonance characteristics using the perturbation method. The findings indicate that simultaneous alterations of PSS parameters can cause critical modes to become unstable, corresponding to strong resonance conditions.

Keywords - Power System Stabilizer, Strong resonance, Participation factor, Multi-model decomposition, Multi-machine.

1. Introduction

To meet the rising load demand, the structure of power systems must be expanded with more sources and interconnections. Also, the parameter settings need changes at the instance to accommodate the ever-changing load. However, an improper parameter setting in dynamic systems can cause an intense collision of oscillatory modes with negative impacts [1]. In recent decades, there has been more attention to the Power System Stabilizer (PSS) design as its improper parameter settings may destabilize the power system due to modal collision. Ensuring the stability and selection of controller parameters for multi-machine power systems are the challenging tasks in today's power system research. The design of distributed PSS with relative rotor speed deviation as the feedback input is proposed in [2]. The results show improved power system stability with increased synchronizing torque.

It is well known that modal resonance has several matching inherent frequency modes. Primarily studied mechanical vibration, focusing on identification, analysis, and control. Power electronics dominate power systems, and modal resonance theory is utilized in thermal power units, renewable energy, and wind power systems to cause wideband oscillations due to dynamics.

Modal resonance in a power system affects damping and controller performance, leading to sensitive eigenvectors or

participation factors. It's crucial for stability analysis and control, and its application has expanded with the development of power electronics. Limited research on strong resonance with PSS. However, multimachine systems require multiple PSS, necessitating future studies on stability and mitigation methods with multiple PSS.

This paper analyses the impact of PSS parameter settings in multi-machine systems. The study system is adapted from an IEEE 3-machine, a 9-bus system with one additional bus (bus-10), PSS connected to any one of the machines. To assess the strong resonance behaviour in PSS design, the modal analysis is performed through the proposed system's full-order and reduced-order models, where the reduced-order model retains only the modes of interest.

The modal decomposition method obtains the reduced-order model with modes of interest. The identification of modes is carried out by the participation factor method. The results show that the trajectory of reduced-order system modes helps determine the tendency of full-order system modes towards instability region during parameter change.

The remaining part of this article is organized into the following sections: Section 2, literature survey; Section 3, mathematical modeling of the multi-machine system; Section 4, modal identification; Section 5, modal analysis on strong resonance; and finally, Section 6, concluding remarks.



2. Literature Survey

The systematic approach of modal analysis using open-loop systems is proposed to calculate the damping and stability of oscillatory modes. The eigenvalue analysis and transient damping torque are validated through simulation analysis. The types of oscillatory modes for a weak grid and the interaction of a weak grid with Inter-inverter-Based Resources (IBR) modes are analyzed in [3]. It is noted that the effect of grid strength is minimal on inter-IBR modes.

In [4, 5], the modal info of open loop subsystems is applied to identify the instability of sub-synchronous oscillations caused by the converter-based wind farms. [6] presents a modal analysis method for the Multi-Input, Multi-Output, closed-loop model with a grid-connected wind farm. [7] examines the mechanism studies of sub-synchronous oscillation incidents in grid-connected wind farms, outlines investigation methods, reviews existing studies, and discusses research gaps. [8] presents a closed-loop interconnected power system model with a voltage source converter-based HVDC line, highlighting the potential mechanism of open-loop modal coupling degrading power system SSOs. Over the past decade, the real-world subsynchronous oscillation events in inverter-based resources have focused on power grid characteristics like series compensation and low system strength [9].

The small-signal stability of an integrated multiterminal DC/AC power system highlights the risk of small-signal instability and its application in parameter tuning for multimachine power systems [10]. Establishment of a Task Force in 2016 to re-observe and encompass the definitions and classifications of power system stability, based on the IEEE PES report, to integrate the outcomes of rapid power electronic devices [11]. In [12], it investigates the damping degradation in a multimachine system, revealing strong dynamic interactions between the generator and the system.

In [13], proposing an open-loop modal analysis method for studying SSOs caused by DFIGs. [14], investigates torsional Sub-Synchronous Oscillations (SSOs) in grid-connected wind farms, revealing open-loop coupling and closed-loop modal repulsion, and proposes a method for detecting instability risk. In [15], the study compares three methods for studying Sub-Synchronous Oscillations (SSOs) in grid-connected wind turbine generators, revealing their limitations and highlighting negative resistance and net damping due to dynamic interactions.

In [16], the study investigates the influence of ineffective grid linking on torsional Sub-Synchronous Oscillations (SSOs), highlighting that it amplifies the modal resonance between DFIG and torsional dynamics. Oscillations in a multimachine power system with multiple wind generators, identifying potential grid connection issues [17]. Analyzed

stability of small-signal synchronization in grid-forming and control parameters [18]. The growing challenges of renewables and power electronics in power systems highlight the need for new classifications and research prospects in this area [19]. In [20], large-scale wind farms highlight each method's strengths and weaknesses. potential mitigation techniques for Sub-Synchronous Control Interaction (SSCI) in wind farms, including active damping controls using flexible AC transmission systems and WTC controls [21].

The historical definitions and classifications of Sub-Synchronous Oscillation (SSO) in grid-connected wind farms discuss recent incidents and propose new terminologies for better understanding [22]. Parallel compensation enhances voltage quality in power grids, but direct-drive wind farms face oscillation risks. Analysis reveals DC voltage outer loop control affects medium-frequency oscillation, while phase-locked loop control affects sub-synchronous oscillation [23].

The mechanism of torsional Sub-Synchronous Oscillations (SSOs) in grid-connected wind farms using near-strong modal resonance proposes a method to detect NESMOR in interconnected subsystems [24]. A robust, efficient, and fast method using Deep Learning and Dissipating Energy Flow to locate forced oscillation sources in large-scale power systems [25]. [26] presents non-stationary forced oscillations, utilizing continuous model detection and signal identification for stability indices and verification in a modified Southeast Australian power system [27], introduces a localization method for identifying forced oscillation disturbance sources in large-scale power systems, improving data privacy, confidentiality, computational performance, and learning efficiency.

The damping power system oscillations, identifying control design techniques, technologies, and characteristics used in power systems, discussing devices, tools, methodology, and technology life cycle [28]. In [29], sub-synchronous control interactions in the induction generator reveal that open-loop modal resonance can weaken the system's damping ability. The power system stability through modal resonance extends from synchronous generator low-frequency resonance to renewable energy wideband oscillation, its hazards, theoretical analysis, and future research [30].

In [31], the impact of participation factors on damping controller configuration in direct-drive wind farms is proposed as a mitigation method and conducts PSCAD/EMTDC simulations. A dynamic equivalent model for analyzing sub-synchronous oscillation in an N-machine wind farm demonstrates its rationality despite a significant reduction in system order [32]. While resonance frequency may be found using resonance modal analysis, nothing is known about the intricate calculation method or how one component relates to the other [33].

3. Mathematical Modeling of Multi-Machine System

The study system is adapted from the IEEE 3-machine 9-bus system with one additional bus (bus-10) as in Figure 1, Neglecting the prime mover dynamics, the electrical dynamics of synchronous machines are modeled as the two-axis model [1]. The three machines are marked as M₁, M₂, and M₃ in Figure 1. In the study system, a single PSS is connected to any of the three machines. The transfer function of PSS [1] is formulated in the form below.

$$\frac{\Delta V_{pss}}{\Delta S_{m_i}} = \frac{K_{pss}(1+sT_1)}{1+sT_2} \quad (1)$$

The time constants T₁, and T₂ are related to center frequency f_c of PSS as follows.

$$f_c = \frac{1}{2\pi\sqrt{T_1T_2}} \quad (2)$$

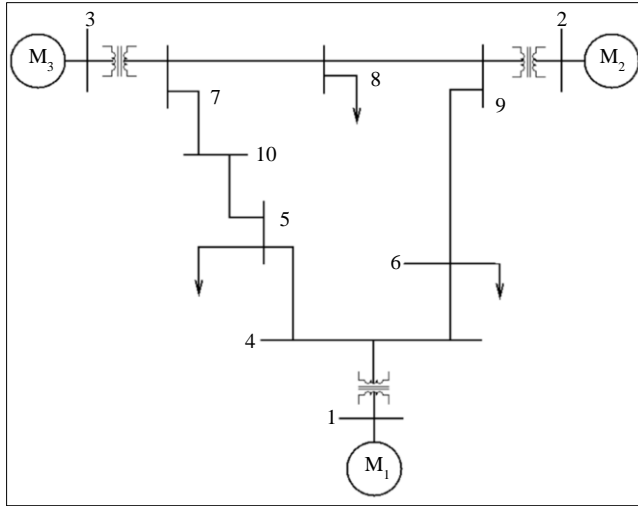


Fig. 1 Study system: schematic layout of three machine power system

3.1. Full-Order System

The linearized model of the study system is developed in MATLAB-Simulink using differential and algebraic equations [1]. The full-order model of the system is represented in the state-space form in Equation (3), and Equation (4).

$$\dot{X} = A_{f_s}X + B_{f_s}u \quad (3)$$

$$y = C_{f_s}X + D_{f_s}u \quad (4)$$

Where:

- u = ΔV_{pss}
- X = Vector of n state variables
- f_s = Full-order system
- u = Input variables of the system
- y = output variables of the system

$$X = \left[\Delta \delta_{m_i}, \Delta S_{m_i}, \Delta E'_{q_j}, \Delta E'_{d_j}, \Delta E'_{fd_j} \right]^t$$

- $\Delta \delta_{m_i}$ = Rotor angle of the i^{th} swing mode
- ΔS_{m_i} = Slip of the i^{th} swing mode
- $\Delta E'_{q_j}$ = Quadrature axis voltage of the j^{th} machine
- $\Delta E'_{d_j}$ = Direct axis voltage of the j^{th} machine
- $\Delta E'_{fd_j}$ = Field excitation voltage of the j^{th} machine

3.2. Reduced-Order System Modeling Using Multi-Modal Decomposition

From the full-order state-space model (Equation (3), Equation (4)), a reduced-order system is obtained by the method of multi-modal decomposition [9, 23]. Arranging the state variables as in Equation (5).

$$X = \left[\Delta \delta_1, \Delta \delta_2, \dots, \Delta \delta_i, \Delta S_{m_1}, \Delta S_{m_2}, \dots, \Delta S_{m_i}, \dots, Z^T \right]^t \quad (5)$$

Where,

- $\Delta \delta$ = Machine angles of the system,
- ΔS_m = Slips of the system,
- Z = Other state variables,
- i = 1 2 3.... etc.

In modal decomposition, a transformation matrix T is defined to transform the full-order system. The modal transformation gives transformed matrices, such as the state variable matrix. $X_m (= T^{-1}X)$ and system matrix A_m is given below.

$$X_m \dot{=} [T^{-1} A_{f_s} T] X_m + T^{-1} B_{f_s} u = [A_m] X_m + [B_m] u \quad (6)$$

Where, A_{m21} is a diagonal matrix, which is denoted by $\Omega (= Q^{-1} A_{f_s21} Q)$. Here, A_{f_s21} is the sub-matrix of A_{f_s} , which relates to rotor angles and slips of the machines. Q is the $i \times i$ size matrix, which is the matrix of the right eigenvectors of A_{f_s21} . The modal frequencies (ω_i) are nearly determined using the relation $\omega_i = \sqrt{\{w_b k_{mi}$ rad/s, where $-k_{mi}$ are the diagonal elements of matrix Ω .

3.3. Single Machine Equivalent Model

To analyze the strong resonance between i^{th} Swing Mode (SM _{i}) and j^{th} machine Exciter Mode (EM _{j}) the state variable equations are arranged in such a way that $\Delta \delta_{mi}$ and ΔS_{mi} are the first and second variables, $\Delta E'_{qj}$ and $\Delta E'_{fdj}$ are the third and fourth variables in the reduced order system. It is adequate to form the reduced system only with those state variables that contribute to strong resonance. The state-space model of the reduced system is given as,

$$X_{rs} \dot{=} A_{rs} X_{rs} + B_{rs} u \quad (7)$$

Where,

rs : Suffices denote the reduced order system.

$$X_{rs} = \left[\Delta \delta_{m_i}, \Delta S_{m_i}, \Delta E'_{q_j}, \Delta E'_{fd_j} \right]^t$$

The reduced system is a single machine connected to an infinite bus system, consisting of rotor swing equations with input from PSS. The single-machine equivalent model comprises the Heffron-Phillips constants. K_1 to K_6 as given below.

$$K_1 = -2 \times H_m \times A_{rs21}, K_4 = -T'_{do} \times A_{rs31}$$

$$K_2 = -2 \times H_m \times A_{rs23}, K_5 = -A_{rs41} \times \frac{T_A}{K_A}$$

$$K_3 = \frac{-1}{T'_{do} \times A_{rs33}}, K_6 = -A_{rs43} \times \frac{T_A}{K_A}$$

Where H_m is the modal inertia at the j^{th} machine to the i^{th} mode, D_m is the modal damping associated with i^{th} mode, T'_{do} is the time constant, K_A is gain, T_A is exciter time constant.

The reduced system is in Equation (8).

$$M\ddot{q} + D\dot{q} + Aq = B(u) \quad (8)$$

Where,

$$u = \Delta V_{pss}$$

$$q = \left[\Delta \delta_{m_i}, \Delta E'_{q_j} \right]^t$$

M, D, A, and B are given in Appendix 1.

The third-order equation is obtained by substituting Equation (1) in the second-order Equation (8).

$$[A_1] \frac{d^3q}{dt^3} + [A_2] \frac{d^2q}{dt^2} + [A_3] \frac{dq}{dt} + [A_4q] = 0 \quad (9)$$

Where the co-efficient matrices A_1 to A_4 are given in appendix 2.

The elements of co-efficient matrices A_1 to A_4 are functions of the parameter vector $[K_{pss}, f_c]$. The strong resonance characteristics of the reduced system are analyzed through the asymptotic trajectory of its hyperbolae. In this computation, the double roots and associated vectors of the characteristic Equation (10) are used to construct hyperbolae, as explained in [5, 9].

$$\det[S^3 A_1 + S^2 A_2 + S A_3 + A_4] = 0 \quad (10)$$

4. Modal Identification

In a multi-machine system, there are several Swing Modes and Exciter Modes. The number of Exciter Modes is as many number of machines; hence, each (EM_j) mode is associated with one machine. Meanwhile, the number of

swing modes is one less than the number of machines. Therefore, it is necessary to identify the contribution of state variables on (EM_j) and (SM_i) modes to associate them with most participating machines. In this section, modal identification is performed using a full-order system through the eigenvalue analysis followed by the participation factor method.

4.1. Eigenvalue Analysis

The eigenvalue analysis is performed with a linearized model of the full-order system developed in MATLAB-Simulink using differential and algebraic equations [1]. Table 1, and Table 2 show the study system's eigenvalue without and with PSS, respectively. The swing and exciter modes are designated in Table 1, and Table 2.

Table 1. Eigenvalues of the study system without PSS

Mode	Eigenvalues	Comments
$\lambda_{1,2}$	$-9.6602 \pm j 19.515$	Exciter Mode #1
$\lambda_{3,4}$	$-10.448 \pm j 13.662$	Exciter Mode #2
$\lambda_{5,6}$	$-11.258 \pm j 11.341$	Exciter Mode #3
$\lambda_{7,8}$	$-0.45098 \pm j 13.157$	Swing Mode #1
$\lambda_{9,10}$	$-0.039361 \pm j 8.5849$	Swing Mode #2
λ_{11}	$-4.3445 + j 0$	-
λ_{12}	$-3.2507 + j 0$	-
λ_{13}	$0.0000 + j 0$	-
λ_{14}	$-0.0063785 + j 0$	-
λ_{15}	$-3.2258 + j 0$	-

Table 2. Eigenvalues of the study system with PSS

Mode	Eigenvalues	Comments
$\lambda_{1,2}$	$-8.068 \pm j 20.142$	Exciter Mode #1
$\lambda_{3,4}$	$-10.256 \pm j 13.164$	Exciter Mode #2
$\lambda_{5,6}$	$-7.239 \pm j 14.167$	Exciter Mode #3
$\lambda_{7,8}$	$-4.164 \pm j 12.509$	Swing Mode #1
$\lambda_{9,10}$	$-0.1752 \pm j 8.5393$	Swing Mode #2
λ_{11}	$-4.3446 + j 0$	-
λ_{12}	$-3.2821 + j 0$	-
λ_{13}	$0.0000 + j 0$	-
λ_{14}	$-0.050149 + j 0$	-
λ_{15}	$-3.2258 + j 0$	-
λ_{16}	$-42.518 + j 0$	-

4.2. Participation Factor Method

The full-order system is used to select the location of PSS by applying the participation factor method. It is to be noted that the speed derivative of that machine, which has the highest participation in a mode, is found to be the best signal to dampen the oscillations due to that mode. The participation factor is computed using equation's left and right eigenvectors (11).

$$P_{jk} = \frac{\|W_{kj}\| \|V_{jk}\|}{\sum_{j=1}^m \|W_{kj}\| \|V_{jk}\|} \quad (11)$$

Where, m is the number of state variables and W and V are the left and right eigenvectors. Table 3, and Table 4 show the absolute values of participation factors in EM_j and SM_i . Modes with PSS are connected to machine-3, respectively.

To find the relative sensitivity of EM_j and SM_i . Modes concerning variation in PSS gain, the participation factor is also computed for different values of K_{pss3}

From Table 3, it is clear that the state variables. $E_{q'}$ and $(E')_{fd}$ of machine-3 is more significant than other variables, as highlighted in bold. Hence, the corresponding mode (EM_3) is associated with machine 3. Similarly, EM_1 and EM_2 are associated to machine-1 and machine-2 respectively.

Further, in Table 4, it is to be seen that the speed derivative of machine-3 is highest in SM_1 . Hence, machine-3 is the best location for PSS to enhance the damping of SM_1 . Similarly, it is found that machine-2 is the best location of PSS to enhance the damping of SM_2 .

5. Modal Analysis on Strong Resonance

In a dynamic system, a complex pair of modes may move in close proximity when at least two independent parameters change. Likewise, the oscillatory modes of the study system, namely Exciter Mode (EM_j) and Swing Mode (SM_i) may move in close proximity when control parameters of PSS change simultaneously.

In the proposed PSS structure, the gain (K_{pss}) and center frequency (f_c) are framed as the design parameters. Accordingly, the strong resonance characteristics of the study are analyzed for change in these two parameters of PSS.

In the following subsection, the modal analysis of strong resonance is performed with a single PSS connected to one of the machines. The root loci of the full-order system are presented to find the direction of movement of EM_j and SM_i in the range of parameter variations.

On the other hand, the asymptotic trajectories of the reduced-order system are plotted by the perturbation method to find the path of EM_j and SM_i in the modal frequency range.

At last, the results of the two approaches are compared to validate the findings about strong resonance.

Table 3. Participation factors of Exciter Modes ($\lambda_{1,2}$, $\lambda_{3,4}$ and $\lambda_{5,6}$) with varying PSS gain (K_{pss3})

Variable	EM ₁	EM ₂	EM ₃	K _{pss3}
$E'_{q'}$	0.4136	0.4682	0.9672	1
$E'_{d'}$	0	0.0153	0.0635	
E'_{fd}	0.3771	0.4647	0.7762	
$E'_{q'}$	0.3365	0.3585	0.4258	5
$E'_{d'}$	0	0.0101	0.0033	
E'_{fd}	0.3245	0.3262	0.3591	
$E'_{q'}$	0.3303	0.3503	0.4032	10
$E'_{d'}$	0	0.0098	0.0025	
E'_{fd}	0.3014	0.3065	0.3439	

Table 4. Participation factors of Swing Modes ($\lambda_{7,8}$ and $\lambda_{9,10}$) with varying PSS gain (K_{pss3})

Variable	SM ₁	SM ₂	K _{pss3}
δ_1	0.0209	0.1453	1
δ_2	0.2163	0.3175	
δ_3	0.8086	0.0785	
S_{m_1}	0.0209	0.1453	
S_{m_2}	0.2163	0.3175	
S_{m_3}	0.8199	0.0663	
δ_1	0.0699	0.1221	5
δ_2	0.0828	0.4405	
δ_3	0.4513	0.0471	
S_{m_1}	0.0699	0.1221	
S_{m_2}	0.0829	0.4406	
S_{m_3}	0.1309	0.0335	
δ_1	0.1138	0.1022	10
δ_2	0.0603	0.4337	
δ_3	0.4292	0.0188	
S_{m_1}	0.1139	0.1022	
S_{m_2}	0.0603	0.4337	
S_{m_3}	0.4292	0.0137	

5.1. Effect of PSS Gain (K_{pss}) Variation

In the study system, machine-1 bus being the reference, the analysis is performed with PSS connected to only one rest of the two machines. When PSS is connected to machine 3, the gain $K_{pss3} = 0.5$ to 20 is varied in this range with small positive perturbation in center frequency ($\Delta f_c > 0$).

Figure 2 shows the root loci of a full-order system with changes in K_{pss3} . From Figure 2, it is observed that the damping of EM_3 decreases with an increase in K_{pss3} , whereas the damping of SM_1 increases.

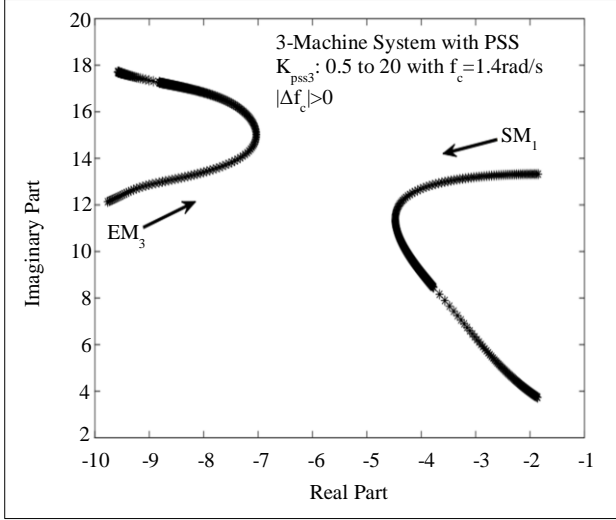


Fig. 2 Root loci of full-order study system with varying gain K_{pss3}

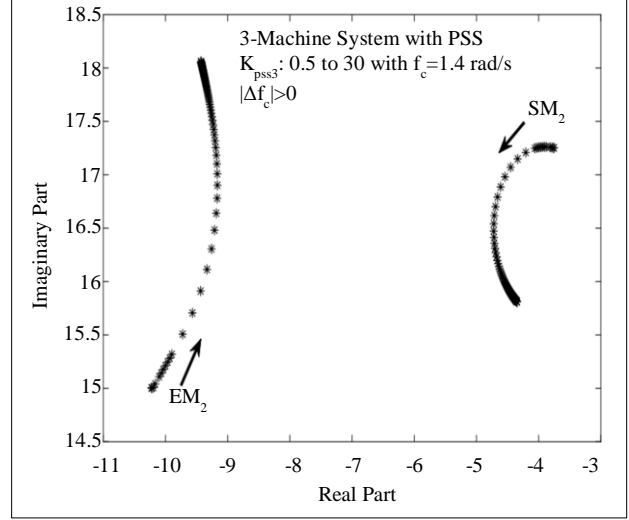


Fig. 4 Root loci of full-order study system with varying gain K_{pss2}

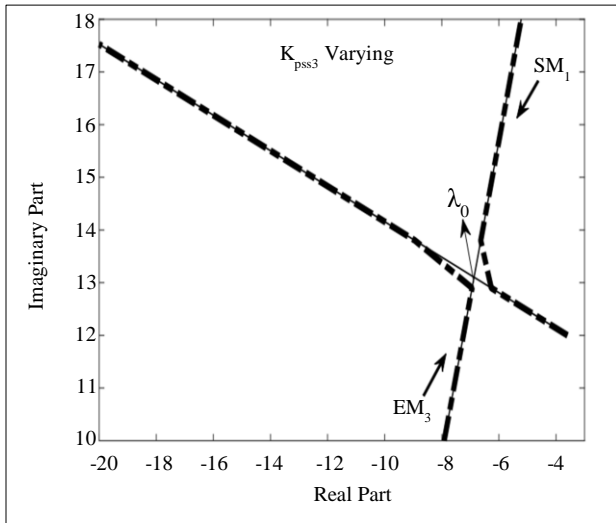


Fig. 3 Asymptotic behavior of modes of reduced-order study system with varying gain K_{pss3}

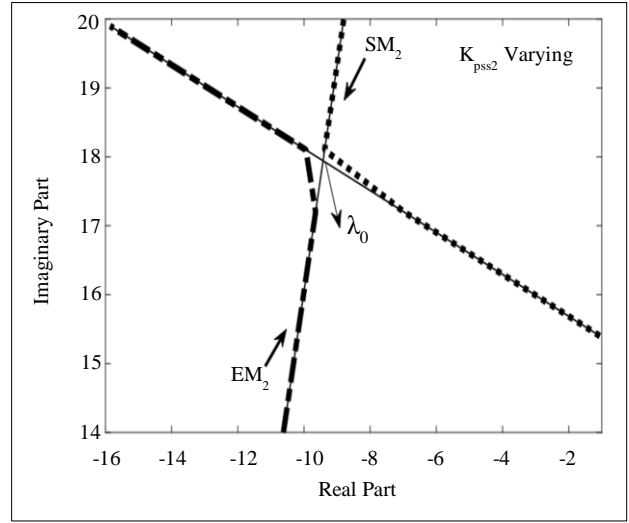


Fig. 5 Asymptotic behavior of reduced-order study system with varying gain K_{pss2}

When the two eigenvalues are nearby, the modes move in opposite directions due to the negative impact of the resonance condition. Therefore, SM_1 moves towards instability region. A similar phenomenon is observed in asymptotic trajectories of reduced-order systems for variation in gain K_{pss3} with $\Delta f_c > 0$, as shown in Figure 3.

In Figure 3, it is observed that the two modes collide and encounter strong resonance at $-7.0549 \pm j 14.7109$, then diverge. Following the strong resonance, SM_1 moves towards the instability region, which is evident from Figure 2 and Figure 3.

When PSS is connected at machine-2, the strong resonance is noted among EM_2 and SM_2 by varying $K_{pss2}=0.5$ to 30. Figure 4 Shows root loci of full-order system with change in K_{pss2} .

In Figure 4, it is to be observed that SM_2 moves towards unstable region followed by proximity of EM_2 and SM_2 . A similar phenomenon is observed in asymptotic trajectories of reduced-order systems for variation in gain K_{pss2} with $\Delta f_c > 0$, as shown in Figure 5. In Figure 5, it is to be observed that the two modes collide with each other and encounter strong resonance at $-7.423 \pm j 17.184$, then diverge. Following the strong resonance, SM_2 moves towards the instability region, as evidenced by Figure 4, and Figure 5.

5.2. Effect of Center Frequency (f_c) Variation

When PSS is connected at machine-3, the center frequency $f_c = 0.8$ to 2 rad/s is varied with $\Delta K_{pss3} > 0$. Figure 6 shows the root loci of the full-order system with changes in f_c . From Figure 6, it is observed that the damping of EM_3 decreases with an increase in K_{pss3} , whereas the damping of SM_1 increases.

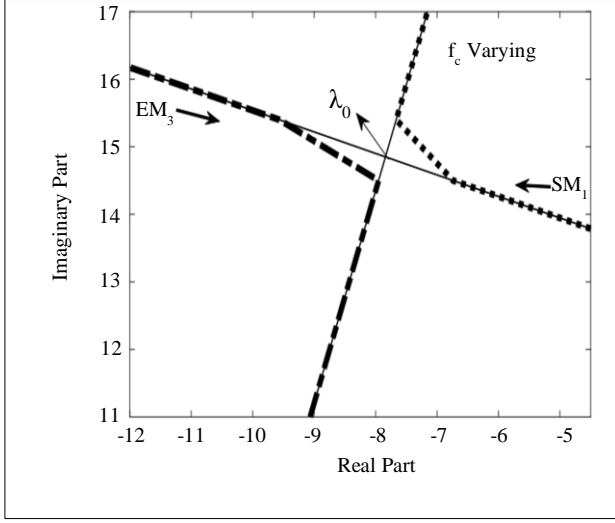


Fig. 6 Root loci of full-order study system with varying f_c on machine-3

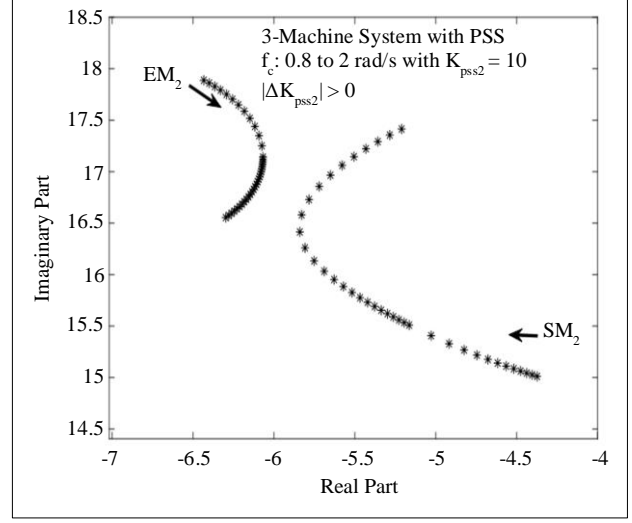


Fig. 8 Root loci of full-order study system with varying f_c on machine-2

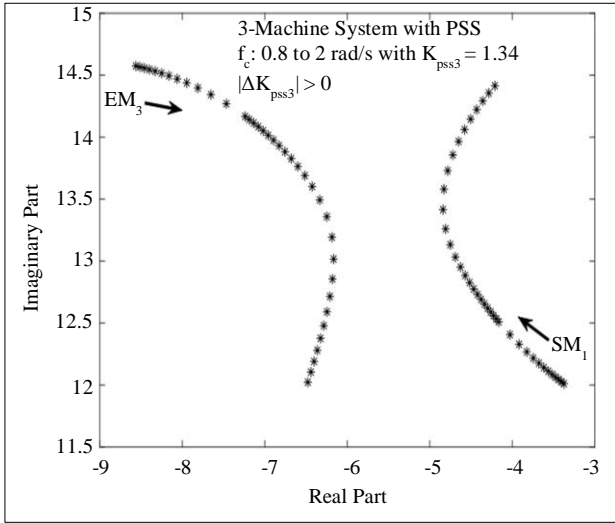


Fig. 7 Asymptotic behavior of reduced-order study system with varying f_c on machine-3

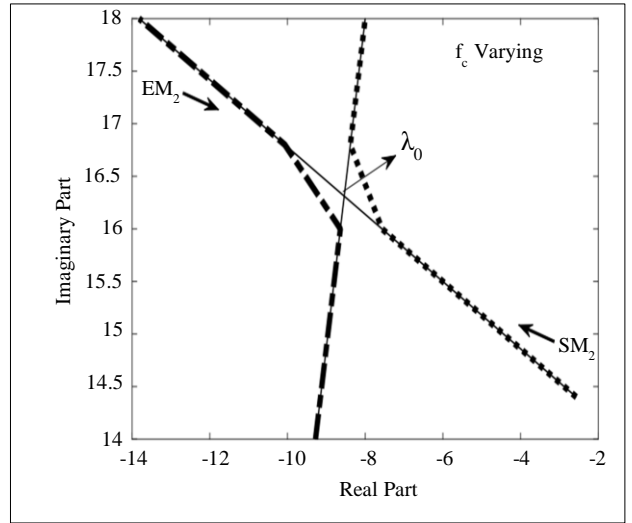


Fig. 9 Asymptotic behavior of reduced-order study system with varying f_c on machine-2

When the two eigenvalues are in close proximity, the modes move in opposite directions due to the negative impact of the resonance condition. Therefore, SM_1 moves towards the unstable region. A similar phenomenon is observed in asymptotic trajectories of a reduced-order system for variation in f_c with $\Delta K_{pss3} > 0$, as shown in Figure 7.

In Figure 7, it is to be noted that both modes collide and encounter strong resonance at $-7.8398 \pm j 14.8773$, then diverge. Following the strong resonance, SM_1 moves towards the instability region, which is evident in Figures 6 and 7. When PSS is connected at machine-2, the strong resonance is observed between EM_2 and SM_2 by varying $f_c = 0.8$ to 2 rad/s. Figure 8 shows the root loci of the full-order system with changes in f_c . In Figure 8, it is to be observed that SM_2 moves towards unstable region followed by proximity of EM_2 and M_2 . A similar phenomenon is observed in asymptotic

trajectories of reduced-order systems for variation in f_c with $\Delta K_{pss2} > 0$, as shown in Figure 9. In Figure 9, it is noticed that both modes collide and encounter strong resonance at $-8.539 \pm j 16.311$, then diverge. Following the strong resonance, SM_2 moves towards the instability region, which is evident from Figure 8 and Figure 9. As $\Delta f_c > 0$ is fixed, ΔK_{pss3} and ΔK_{pss2} are varied independently, two modes collide and encounter strong resonance at frequencies of $\pm j 14.7109 \pm j 17.184$ rad/sec, respectively. EM is stabilized, whereas SM is destabilized. When Δf_c is varied, $\Delta K_{pss3} > 0$ and $\Delta K_{pss2} > 0$ are fixed independently; two modes collide and encounter strong resonance at frequencies of $\pm j 14.8773 \pm j 16.311$ rad/sec, respectively. EM is destabilized, and SM is being stabilized. The performance of strong resonance is consistent across full-order and reduced-order systems, indicating that one mode turns unstable after the strong resonance.

6. Conclusion

This paper examines the dynamics of strong resonance in a multi-machine system when a single Power System Stabilizer (PSS) is connected to a machine. In addition, some of the findings and indications of the system behavior observed during the analysis are.

- i) The study observes the interaction between the swing mode and the exciter mode of the generator while adjusting the PSS gain and center frequency.
- ii) The study conducts full-order and reduced-order system analyses to observe mode behavior pre and post-strong resonance encounters.

- iii) Utilizes participation factor analysis on the speed derivative of the machine to determine the optimal damping signal.
- iv) The root locus plots (for the full-order model) and asymptotic plots (for the reduced-order system) indicate that the swing mode tends towards instability after encountering strong resonance.
- v) Strong resonance is a potential phenomenon to induce system destabilization.

Limited research on strong resonance with PSS. However, multimachine systems require multiple PSS, necessitating future studies on stability and mitigation methods with multiple PSS.

References

- [1] K.R. Padiyar, *Power System Dynamics: Stability and Control*, 2nd ed., Anshan, 2004. [[Google Scholar](#)] [[Publisher Link](#)]
- [2] Ganggang Tu et al., "Distributed Power System Stabilizer for Multimachine Power Systems," *IET Generation, Transmission, and Distribution*, vol. 13, no. 5, pp. 603-612, 2019. [[CrossRef](#)] [[Google Scholar](#)] [[Publisher Link](#)]
- [3] Lingling Fan, "Inter-IBR Oscillation Modes," *IEEE Transactions on Power Systems*, vol. 37, no. 1, pp. 824-827, 2022. [[CrossRef](#)] [[Google Scholar](#)] [[Publisher Link](#)]
- [4] Wenjuan Du, Bixing Ren, and Haifeng Wang, "Approximate Model-Free Assessment of Oscillation Stability Determined by the PLLs in a Weakly Grid-Connected Wind Farm with Multiple PMSGs," *Electric Power Components and Systems*, vol. 48, no. 6-7, pp. 742-753, 2020. [[CrossRef](#)] [[Google Scholar](#)] [[Publisher Link](#)]
- [5] Wenjuan Du et al., "Sub-Synchronous Oscillations Caused by Grid-Connected PMSGs under the Condition of Near Strong Open-Loop Modal Resonance," *Electric Power Components and Systems*, vol. 47, no. 19-20, pp. 1731-1743, 2019. [[CrossRef](#)] [[Google Scholar](#)] [[Publisher Link](#)]
- [6] Wenjuan Du et al., "Open-Loop Modal Analysis to Identify the SSO Instability Risk Caused by Grid Connected Wind Farms," *International Journal of Electrical Power & Energy Systems*, vol. 107, pp. 352-362, 2019. [[CrossRef](#)] [[Google Scholar](#)] [[Publisher Link](#)]
- [7] Chen Chen et al., "Sub-Synchronous Oscillations in Power Systems Caused by Grid-Connected Wind Farms -A Survey of Mechanism Studies," *CSEE Journal of Power and Energy Systems*, vol. 4, no. 4, pp. 495-503, 2018. [[CrossRef](#)] [[Google Scholar](#)] [[Publisher Link](#)]
- [8] Wenjuan Du, Qiang Fu, and Haifeng Wang, "Subsynchronous Oscillations Caused by Open-Loop Modal Coupling between VSC-Based HVDC Line and Power System," *IEEE Transactions on Power Systems*, vol. 33, no. 4, pp. 3664-3677, 2018. [[CrossRef](#)] [[Google Scholar](#)] [[Publisher Link](#)]
- [9] Yunzhi Cheng et al., "Real-World Subsynchronous Oscillation Events in Power Grids with High Penetrations of Inverter-Based Resources," *IEEE Transactions on Power Systems*, vol. 38, no. 1, pp. 316-330, 2023. [[CrossRef](#)] [[Google Scholar](#)] [[Publisher Link](#)]
- [10] Wenjuan Du et al., "Open-Loop Modal Coupling Analysis for a Multi-Input Multi-Output Interconnected MTDC/AC Power System," *IEEE Transactions on Power Systems*, vol. 34, no. 1, pp. 246-256, 2019. [[CrossRef](#)] [[Google Scholar](#)] [[Publisher Link](#)]
- [11] Nikos Hatziaargyriou et al., "Definition and Classification of Power System Stability - Revisited & Extended," *IEEE Transactions on Power Systems*, vol. 36, no. 4, pp. 3271-3281, 2021. [[CrossRef](#)] [[Google Scholar](#)] [[Publisher Link](#)]
- [12] Wenjuan Du, Jingtian Bi, and Haifeng Wang, "Damping Degradation of Power System Low-Frequency Electromechanical Oscillations Caused by Open-Loop Modal Resonance," *IEEE Transactions on Power Systems*, vol. 33, no. 5, pp. 5072-5081, 2018. [[CrossRef](#)] [[Google Scholar](#)] [[Publisher Link](#)]
- [13] Wenjuan Du et al., "Concept of Modal Repulsion for Examining the Sub-Synchronous Oscillations in Power Systems," *IEEE Transactions on Power Systems*, vol. 33, no. 4, pp. 4614-4624, 2018. [[CrossRef](#)] [[Google Scholar](#)] [[Publisher Link](#)]
- [14] Wenjuan Du et al., "Concept of Modal Repulsion for Examining the Subsynchronous Oscillations Caused by Wind Farms in Power Systems," *IEEE Transactions on Power Systems*, vol. 34, no. 1, pp. 518-526, 2019. [[CrossRef](#)] [[Google Scholar](#)] [[Publisher Link](#)]
- [15] Wenjuan Du et al., "Comparison of Methods to Examine Sub-Synchronous Oscillations Caused by Grid-Connected Wind Turbine Generators," *IEEE Transactions on Power Systems*, vol. 34, no. 6, pp. 4931-4943, 2019. [[CrossRef](#)] [[Google Scholar](#)] [[Publisher Link](#)]
- [16] Wenjuan Du et al., "Analytical Examination on the Amplifying Effect of Weak Grid Connection for the DFIGs to Induce Torsional Sub-Synchronous Oscillations," *IEEE Transactions on Power Delivery*, vol. 35, no. 4, pp. 1928-1938, 2020. [[CrossRef](#)] [[Google Scholar](#)] [[Publisher Link](#)]
- [17] Wenjuan Du, Xiao Chen, and Haifeng Wang, "A Method of Open-Loop Modal Analysis to Examine the SSOs in a Multi-Machine Power System with Multiple Variable-Speed Wind Generators," *IEEE Transactions on Power Systems*, vol. 33, no. 4, pp. 4297-4307, 2018. [[CrossRef](#)] [[Google Scholar](#)] [[Publisher Link](#)]

- [18] Guangyu Wang et al., “Small-Signal Synchronization Stability of Grid-Forming Converter Influenced by Multi-Time-Scale Control Interaction,” *Energy Reports*, vol. 9, pp. 597-606, 2023. [[CrossRef](#)] [[Google Scholar](#)] [[Publisher Link](#)]
- [19] Jan Shair et al., “Power System Stability Issues, Classifications, and Research Prospects in the Context of High-Penetration of Renewables and Power Electronics,” *Renewable and Sustainable Energy Reviews*, vol. 145, 2021. [[CrossRef](#)] [[Google Scholar](#)] [[Publisher Link](#)]
- [20] Jan Shair et al., “Modeling and Stability Analysis Methods for Investigating Subsynchronous Control Interaction in Large-Scale Wind Power Systems,” *Renewable and Sustainable Energy Reviews*, vol. 135, 2021. [[CrossRef](#)] [[Google Scholar](#)] [[Publisher Link](#)]
- [21] Jan Shair, Xiaorong Xie, and Gangui Yan, “Mitigating Subsynchronous Control Interaction in Wind Power Systems: Existing Techniques and Open Challenges,” *Renewable and Sustainable Energy Reviews*, vol. 108, pp. 330-346, 2019. [[CrossRef](#)] [[Google Scholar](#)] [[Publisher Link](#)]
- [22] Jan Shair et al., “Overview of Emerging Subsynchronous Oscillations in Practical Wind Power Systems,” *Renewable and Sustainable Energy Reviews*, vol. 99, pp. 159-168, 2019. [[CrossRef](#)] [[Google Scholar](#)] [[Publisher Link](#)]
- [23] Bingbing Shao et al., “Medium-Frequency and Sub-Synchronous Oscillation Analysis of Direct-Drive Wind Farms Connected to the Parallel-Compensated AC Grid,” *Electric Power Systems Research*, vol. 216, 2023. [[CrossRef](#)] [[Google Scholar](#)] [[Publisher Link](#)]
- [24] Wenjuan Du, Yang Wang, and Haifeng Wang, “Torsional Subsynchronous Oscillations Caused by Grid-Connected Wind Farms in a Complex Multi-Machine Power System under the Condition of Near Strong Modal Resonance,” *Electric Power Systems Research*, vol. 179, 2020. [[CrossRef](#)] [[Google Scholar](#)] [[Publisher Link](#)]
- [25] Mustafa Matar et al., “Transformer-Based Deep Learning Model for Forced Oscillation Localization,” *International Journal of Electrical Power & Energy Systems*, vol. 146, 2023. [[CrossRef](#)] [[Google Scholar](#)] [[Publisher Link](#)]
- [26] Tossaporn Surinkaew et al., “A Unified Damping Controller for Non-Stationary Forced Oscillation,” *International Journal of Electrical Power & Energy Systems*, vol. 143, 2022. [[CrossRef](#)] [[Google Scholar](#)] [[Publisher Link](#)]
- [27] Shuang Feng et al., “A Two-Stage Deep Transfer Learning for Localization of Forced Oscillations Disturbance Source,” *International Journal of Electrical Power & Energy Systems*, vol. 135, 2022. [[CrossRef](#)] [[Google Scholar](#)] [[Publisher Link](#)]
- [28] Zimran Rafique et al., “Bibliographic Review on Power System Oscillations Damping: An Era of Conventional Grids and Renewable Energy Integration,” *International Journal of Electrical Power & Energy Systems*, vol. 136, 2022. [[CrossRef](#)] [[Google Scholar](#)] [[Publisher Link](#)]
- [29] Wenjuan Du, Yang Wang, and H.F. Wang, “Strong Sub-Synchronous Control Interactions Caused by Open-Loop Modal Resonance between the DFIG and Series-Compensated Power System,” *International Journal of Electrical Power & Energy Systems*, vol. 102, pp. 52-59, 2018. [[CrossRef](#)] [[Google Scholar](#)] [[Publisher Link](#)]
- [30] Bingbing Shao et al., “Review on Power System Generalized Modal Resonance Analysis,” *International Journal of Electrical Power & Energy Systems*, vol. 154, 2023. [[CrossRef](#)] [[Google Scholar](#)] [[Publisher Link](#)]
- [31] Bingbing Shao et al., “Analysis and Mitigation of Participation Factors Weak Robustness in Direct-Drive Wind Farms Connected to VSC-HVDC System,” *International Journal of Electrical Power & Energy Systems*, vol. 153, 2023. [[CrossRef](#)] [[Google Scholar](#)] [[Publisher Link](#)]
- [32] Bingbing Shao et al., “An Equivalent Model for Sub-Synchronous Oscillation Analysis in Direct-Drive Wind Farms with VSC-HVDC Systems,” *International Journal of Electrical Power & Energy Systems*, vol. 125, 2021. [[CrossRef](#)] [[Google Scholar](#)] [[Publisher Link](#)]
- [33] Xing Sun, Wanjun Lei, and Yuqi Dai, “Improved Implementation and Analysis of Modal Frequency Sensitivity,” *2021 IEEE 4th International Electrical and Energy Conference (CIEEC)*, Wuhan, China, pp. 1-5, 2021. [[CrossRef](#)] [[Google Scholar](#)] [[Publisher Link](#)]

Appendix 1

$$M = \begin{bmatrix} \frac{2H_m}{\omega_B} & 0 \\ 0 & T_A T'_{do} K_3 \end{bmatrix}$$

$$D = \begin{bmatrix} \frac{D_m}{\omega_B} & 0 \\ K_3 K_4 T_A & T_A T'_{do} K_3 \end{bmatrix}$$

$$A = \begin{bmatrix} K_1 & K_2 \\ K_3(K_4 + K_A K_5) & (1 + K_A K_3 K_6) \end{bmatrix}$$

$$B = \begin{bmatrix} T_m \\ K_3 K_E (\Delta V_s + \Delta V_{ref}) \end{bmatrix}$$

Appendix 2

$$A_1 = \begin{bmatrix} 0 & 0 \\ 0 & \frac{T_E T'_{do} T_2}{K_E} \end{bmatrix}$$

$$A_2 = \begin{bmatrix} \frac{2H_m}{\omega_B} & \frac{2H_m}{\omega_B} \\ \frac{K_4 T_E T_2}{K_E} - K_s T_1 \omega_B & \frac{T_E T_2}{K_3 K_E} + \frac{T'_{do} T_2}{K_E} + \frac{T_E T'_{do}}{K_E} \end{bmatrix}$$

$$A_3 = \begin{bmatrix} \frac{D_m}{\omega_B} & 0 \\ K_5 T_2 + \frac{K_4 T_2}{K_E} - K_s \omega_B + \frac{K_4 T_E}{K_E} & K_6 T_2 + \frac{T_2}{K_E K_3} + \frac{T_E}{K_3 K_E} + \frac{T'_{do}}{K_E} \end{bmatrix}$$

$$A_4 = \begin{bmatrix} K_1 & K_2 \\ K_5 + \frac{K_4}{K_E} & K_6 + \frac{1}{K_3 K_E} \end{bmatrix}$$